BEILSTEIN JOURNAL OF NANOTECHNOLOGY

Improving the catalytic activity for hydrogen evolution of monolayered $SnSe_{2(1-x)}S_{2x}$ by mechanical strain

Sha Dong and Zhiguo Wang*

Full Research Paper

Open Access

Address:
School of Electronics Science and Engineering, Center for Public Security Technology Research, University of Electronic Science and Technology of China, Chengdu, 610054, P.R. China

Email:
Zhiguo Wang* - zgwang@uestc.edu.cn

* Corresponding author

Keywords:
density functional theory (DFT); electronic properties; hydrogen evolution reaction; mechanical strain; $SnSe_{2(1-x)}S_{2x}$ monolayer

Beilstein J. Nanotechnol. **2018,** *9,* 1820–1827.
doi:10.3762/bjnano.9.173

Received: 22 January 2018
Accepted: 29 May 2018
Published: 18 June 2018

Associate Editor: R. Xu

Abstract

Exploring efficient electrocatalysts for hydrogen production with non-noble metals and earth-abundant elements is a promising pathway for achieving practical electrochemical water splitting. In this work, the electronic properties and catalytic activity of monolayer $SnSe_{2(1-x)}S_{2x}$ (x = 0–1) under compressive and tensile strain were investigated using density functional theory (DFT) computations. The results showed $SnSe_{2(1-x)}S_{2x}$ alloys with continuously changing bandgaps from 0.8 eV for $SnSe_2$ to 1.59 eV for SnS_2. The band structure of a $SnSe_{2(1-x)}S_{2x}$ monolayer can be further tuned by applied compressive and tensile strain. Moreover, tensile strain provides a direct approach to improve the catalytic activity for the hydrogen evolution reaction (HER) on the basal plane of the $SnSe_{2(1-x)}S_{2x}$ monolayer. SnSeS and $SnSe_{0.5}S_{1.5}$ monolayers showed the best catalytic activity for HER at a tensile strain of 10%. This work provides a design for improved catalytic activity of the $SnSe_{2(1-x)}S_{2x}$ monolayer.

Introduction

Hydrogen is a clean energy source with outstanding properties such as high specific energy per mass, easy storage and transportation, and ability to reduce harmful emissions [1,2]. Hydrogen is not naturally available as a ready-to-use substance; however, hydrogen can be produced anywhere across the planet through many approaches. Among the approaches used in the mass production of hydrogen, water electrolysis is a clean and "green" approach [3-7]. Efficient electrocatalysts for the hydrogen evolution reaction (HER) with high conversion efficiency are essential for the continuous generation of hydrogen. The platinum (Pt) group materials are regarded as the best electrocatalysts for HER; however, the high cost and limited resources of these types of catalyst restrict their usage in the mass production of hydrogen [8-10]. Therefore, exploring non-noble and earth-abundant elements as catalysts for hydrogen production is one of the most promising pathways for the mass production of hydrogen.

Two-dimensional (2D) atomic layer thin materials, such as monolayer transition-metal dichalcogenides (TMDs) [11-19], have demonstrated many fascinating properties, including the substitution of Pt as an electrocatalyst for HER. 2D MoS_2 has

been widely studied. Recently, tin dichalcogenides SnX_2 (X = S, Se) have also received considerable attention in a variety of fields because of their low cost, use of earth-abundant resources and environmental friendliness [18,20-23]. Monolayer SnX_2 has a X–Sn–X sandwich-like structure, which can be easily synthesized by using traditional mechanical exfoliation techniques [24,25] because of the weak van der Waals (vdW) interactions between layers. These mono- and few-layer SnX_2 (X = S, Se) compounds are expected to be widely used in the fields of water splitting [26], high-speed photodetection [27], electronics [28], and catalysis [29], as well as in the fabrication of solar cells and film electrodes [30].

A good electro-catalyst for HER should have sufficient active sites for catalysis. Furthermore, because electrons participate in the HER process, an ideal catalyst for HER should have good electronic conductivity. Tuning the band structure of the catalyst is important for improving the HER efficiency. It was reported that the band structure and carrier mobility of monolayer MX_2 can be tuned by substitution of M with M' atoms or X with X' atoms to form monolayer $M_xM'_{(1-x)}X_2$ or $MX_{2x}X'_{2(1-x)}$ alloys [31-37]. For example, Komsa et al. [34] have investigated the electronic properties of monolayer $MoS_{2x}Se_{2(1-x)}$ and found that the bandgaps can be continuously tuned with the variation of Se composition. Liu et al. [38] have studied $Mo_{1-x}W_xS_2$ and observed variations of the direct bandgap between 1.85 and 1.99 eV by varying x from 0 to 1. Other 2D-TMDs alloy nanosheets, such as $Mo_{1-x}W_xSe_2$ [39] and $WS_{2(1-x)}Se_{2x}$ [40,41], have also shown tuneable bandgaps and different electrical properties by varying the value of x. Monolayer SnS_2 and $SnSe_2$ have indirect bandgaps of 2.1 and 1.1 eV, respectively. Theoretically, alloying SnS_2 and $SnSe_2$ may yield tuneable bandgaps [36]. Wang et al. [35] have studied the 2D $SnSe_{2(1-x)}S_{2x}$ alloys that were alloyed using chemical vapour transport (CVT) reactions.

Apart from alloying, strain can also be used to tune the electronic properties of nanomaterials. Yue et al. [42] investigated the electronic properties of monolayer MoS_2 under elastic strain and found that the direct-to-indirect transition of MoS_2 occurs at a strain of 0.01, and the semiconductor-to-metal transition occurs at a strain of 0.10. Huang et al. [22] reported that both compressive (−11%) and tensile (14%) strain can trigger the semiconductor–metal transition in the $SnSe_2$ monolayer. Furthermore, Scalise et al. [15] showed that the electronic structure of the MoS_2 monolayer can be reversibly tuned from direct to indirect by applying strain (ca. 2%).

Much research effort has been devoted in recent decades to the development of inexpensive catalysts for the electrochemical HER. Some of the recent studies have focused on monolayer SnX_2 (X = S, Se). Liu et al. [43] investigated SnS_2 nanosheets regarding their electrochemical behaviour and electrocatalytic properties for HER by examining trace amounts of Pt nanoparticles interacting with defect-rich SnS_2; the results demonstrated that SnS_2 may offer new perspectives regarding a utilization in HER. The catalytic activity for HER shows great dependence on the electronic structure of the catalyst. As alloying and strain can be used to tune the electronic properties of the catalyst, they will affect the catalytic behaviour. Several TMD alloy systems have been investigated as catalysts for HER, including $Mo_{1-x}W_xSe_2$ nanoflowers [44], $WS_{2(1-x)}Se_{2x}$ nanotubes [45] and $MoS_{2(1-x)}Se_{2x}$ nanobelts [46]. It was reported that alloying provides an opportunity to tune the Gibbs free energy (ΔG_H) for hydrogen adsorbed on the monolayer alloys and can be used to enhance HER performance. The HER catalytic properties of the catalyst can also be tuned through strain [42,47-52]. Gao et al. [53] demonstrated that a tensile strain is able to strengthen the hydrogen binding on graphitic carbon nitride (g-C_3N_4), whereas compressive strain had the opposite effect. Yan et al. [49] showed that large elastic strains influence the catalytic activity of WC for HER.

Very recently, 2D $SnSe_{2(1-x)}S_{2x}$ alloys have been synthesized experimentally [35]. To our knowledge, theoretical studies related to the system of 2D $SnSe_{2(1-x)}S_{2x}$ alloys as catalysts for HER have been reported rarely. Tuning the electronic properties and catalytic behaviour of $SnSe_{2(1-x)}S_{2x}$ monolayers for HER by strain engineering is required for their application in the energy conversion field. In this work, the electronic properties and catalytic behaviour for HER of $SnSe_{2(1-x)}S_{2x}$ (x = 0, 0.125, 0.25, 0.375, 0.5, 0.625, 0.750, 0.875 and 1.0) monolayers were investigated by density functional theory (DFT). It was shown that band gap and catalytic activity of these alloys can be continuously tuned by strain engineering.

Results and Discussion

2D monolayer TMD is a three-atomic thickness structure with one transition-metal atom layer sandwiched by two chalcogen atom layers. A triangular prism or octahedron can be formed as the transition-metal atom is bonded with six chalcogen atoms, and the former and latter structures are often termed as 2H-phase and 1T-phase, respectively. The stable phase for monolayer SnS_2 is the 1T-phase. Alloying is an efficient approach to tune the electronic properties of semiconductors. Because of the large difference of bandgaps between $SnSe_2$ and SnS_2, the $SnSe_{2(1-x)}S_{2x}$ semiconductor offers wide and continuously fine-tuneable bandgaps when varying the alloy fractions. All the simulations were performed in a 2 × 2 supper cell, which includes 8 S atoms. As 0–8 S atoms are substituted by Se atoms, the monolayer $SnSe_{2(1-x)}S_{2x}$ alloys with x = 0–1 are formed. For each given S content, all possible configurations of

the substitution of S by Se atoms in monolayer SnS_2 are tested; the configuration with the lowest energy was used to model the monolayer $SnSe_{2(1-x)}S_{2x}$, which is different from random structure used in [36]. The electronic properties and catalytic behaviour for HER of the $SnSe_{2(1-x)}S_{2x}$ monolayer are all performed for the energy-stable configuration. The cross and side views of monolayer SnSeS are shown in Figure 1a and Figure 1b, respectively. Sn, S, and Se atoms are presented by brown, yellow, and green balls, respectively. For the monolayer SnSeS, S and Se atoms are preferably distributed orderly. As the size of the S atom is different from that of Se atom, the lattice constant of $SnSe_{2(1-x)}S_{2x}$ monolayer changes with the Se content. Figure 1c shows the variation of the lattice constant as a function of the Se content as x increases from 0 to 1. The lattice constant decreases from 3.87 Å for $SnSe_2$ to 3.70 Å for SnS_2. The calculated lattice constants of 3.87 and 3.70 Å agree with the reported values of 3.89 Å for $SnSe_2$ and 3.70 Å for SnS_2 [35]. The lattice constant shows a linear variation with Se content, which obeys Vegard's law [54] and agrees well with previous results [36].

SnS_2 and $SnSe_2$ monolayers are indirect-bandgap semiconductors, as highlighted in their band structures shown in Figure 1e and Figure 1i, respectively. The valence-band maximum (VBM) is located at the M-point, whereas the conduction-band minimum (CBM) is located at the Γ-point. The band gaps are 1.59 eV for the SnS_2 monolayer and 0.80 eV for the $SnSe_2$ monolayer, in agreement with the previous reported values of 1.60 eV and 0.81 eV, respectively [35]. The band structures of monolayer $SnSe_{2(1-x)}S_{2x}$ with x equal to 0.75, 0.50 and 0.25 are shown in Figure 1f, Figure 1g and Figure 1h, respectively. The substitution of S with Se does not affect the indirect bandgap semiconducting characteristics; however, the band gap is tuned with changing the content of Se, as shown in Figure 1d with the indirect band gap decreasing with increasing Se content. These results agree with the reported by Huang et al. [36] with random $SnSe_{2(1-x)}S_{2x}$ alloys. The bandgap evolution of monolayer $SnSe_{2(1-x)}S_{2x}$ shows a band-bowing effect [36].

There are three possible adsorption sites for hydrogen on pristine SnS_2 and $SnSe_2$ monolayers, i.e., the top of the Sn site, the centre of a hexagonal site, and the top of S/Se atoms. Because of the symmetry breaking in $SnSe_{2(1-x)}S_{2x}$ monolayers, the number of possible adsorption sites is increased. For example, there are six adsorption sites for hydrogen on the SnSeS monolayer, as shown in Figure 2, i.e., the top of S (T_S) and Se (T_{Se}) atoms, two tops of the Sn sites (T1 and T2), and two centres of the hexagonal sites (H1 and H2). The hydrogen is bounded to two S atoms and one Se atom at the T1 and H1 sites, whereas it is bounded to one S atom and two Se atoms at the T2 and H2 sites. After full relaxation, the T and H sites are not energetically stable adsorption sites for hydrogen, which will be relaxed to near the S or Se atoms. Thus, we considered the sites on top of the S and Se atoms as adsorption sites for hydrogen in the following part of this paper.

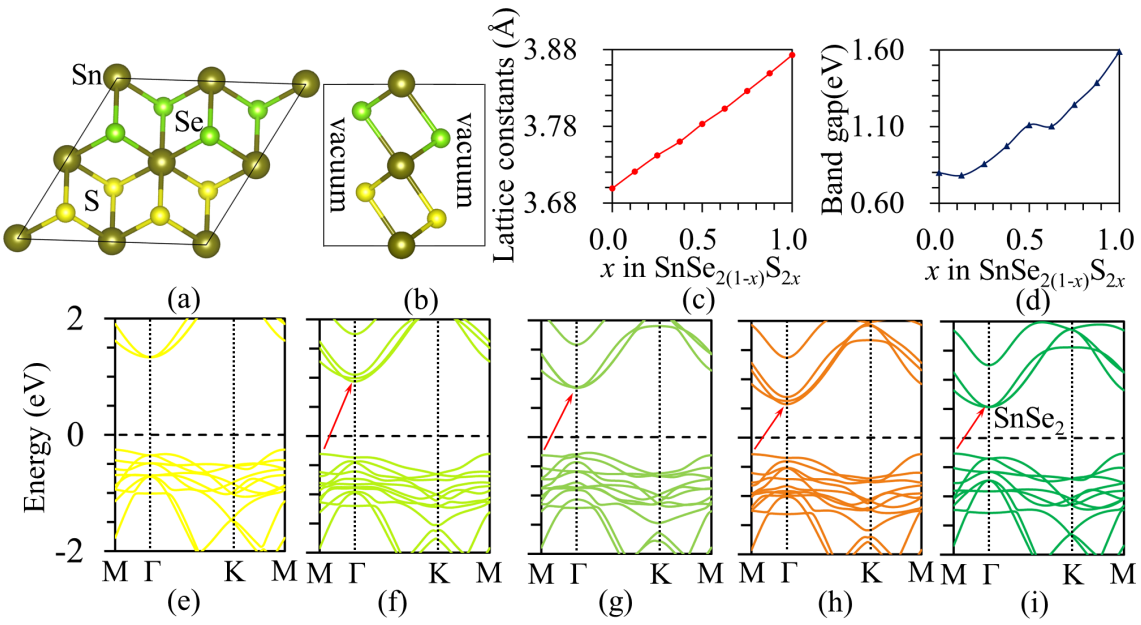

Figure 1: (a) Top view and (b) side view of monolayer SnSeS. (c) Variation of the lattice constant as a function of Se content in monolayer $SnSe_{2(1-x)}S_{2x}$. (d) Band gaps as a function of Se content in monolayer $SnSe_{2(1-x)}S_{2x}$. (e–i) The band structures of monolayer $SnSe_{2(1-x)}S_{2x}$ with x equal to (e) 1.0, (f) 0.75, (g) 0.50, (h) 0.25 and (i) 0.0. The arrows indicate the indirect band gap for a given system.

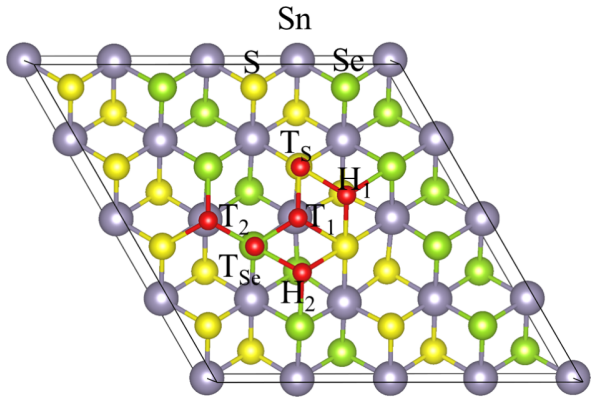

Figure 2: Atom configuration of possible adsorption sites for hydrogen on the SnSeS monolayer.

The Gibbs free energies of hydrogen adsorption on the basal plane of the monolayer of SnS_2 and $SnSe_2$ are 1.08 and 0.96 eV, respectively. Although the Gibbs free energies of hydrogen adsorption at on top of Se and S atoms decrease with increasing the Se content in the $SnSe_{2(1-x)}S_{2x}$ monolayer, the values of ΔG_H are 0.99 and 0.61 eV on top of Se and S atoms, respectively, in the $SnSe_{1.75}S_{0.25}$ monolayer. The large positive values of ΔG_H indicate that hydrogen has a weak interaction with the substrate and is not easily adsorbed on the catalyst. Thus, the basal plane of $SnSe_{2(1-x)}S_{2x}$ monolayer remains chemically inert for HER.

As shown in Figure 3a, biaxial strains ranging from −5% to 10% were applied in the $SnSe_{2(1-x)}S_{2x}$ monolayer to modify the catalytic performance. Strained $SnSe_{2(1-x)}S_{2x}$ monolayer are obtained by varying the lattice value with strain ε (ε = −0.05, −0.03, −0.01, 0.02, 0.03, 0.05, 0.06 and 1.00), i.e., the lattice constant is $a = a_0(1 + \varepsilon)$, where a_0 is the lattice constant without strain. The value of ΔG_H for hydrogen absorbed on $SnSe_{2(1-x)}S_{2x}$ monolayers increases with compressive strains. The values of ΔG_H were calculated to be 0.84 and 1.16 eV in the SnSeS monolayer for hydrogen adsorbed on top of S and Se atoms, respectively, and these values increased to 1.28 and 1.63 eV, respectively, under a compressive strain of −5%. Thus, compressive strain is not helpful for improving the catalytic performance of the $SnSe_{2(1-x)}S_{2x}$ monolayers. With tensile strain applied, the value of ΔG_H decreases with increasing the tensile strain. The values of ΔG_H decrease from 0.84 to −0.05 eV and from 1.16 to 0.18 eV for hydrogen adsorbed on top of the S atom and the Se atom, respectively, in the SnSeS monolayer as the tensile strain increases from 0% to 10%. For the $SnSe_{2(1-x)}S_{2x}$ monolayer with x in the range between 0.25 and 1.00, the values of ΔG_H for hydrogen adsorbed the top of S are close to zero at a tensile strain of 10%; thus, strain can be used to improve the catalytic activity for HER.

As shown in Figure 4, also the band gaps show great dependence on the applied strain. The band gap decreases from 1.59 to 1.48 eV for the SnS_2 monolayer as the compressive strain increases from 0% to −5%, whereas it decreases from 1.59 to 0.90 eV as the tensile strain increases from 0% to 10%. The results indicates that the strain can be used to tune the band gaps of the $SnSe_{2(1-x)}S_{2x}$ monolayers.

These effects may create new opportunities in some specific applications, such as bandgap engineering and device structures. It was reported that the catalytic activity for HER of the monolayer 1T'-MX_2 (M = Mo, W; X = S, Se, Te) can be enhanced by applying tensile strain [55,56]. For 1T'-MoS_2, it was found that the strong hybridization between Mo d-orbitals and S p-orbitals

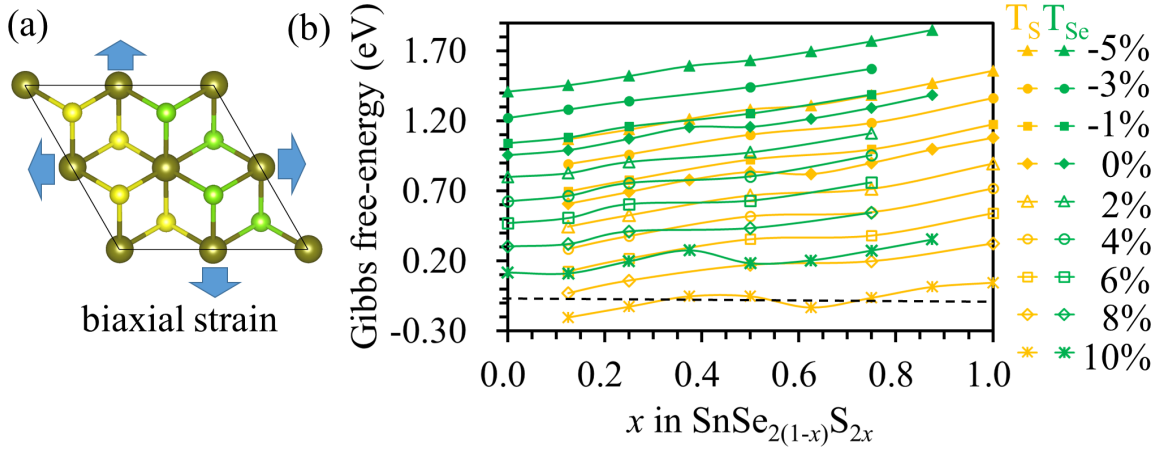

Figure 3: (a) A schematic diagram showing strain applied to $SnSe_{2(1-x)}S_{2x}$ monolayer. (b) Evolution of ΔG_H for the $SnSe_{2(1-x)}S_{2x}$ monolayer with mechanical strain. The black dashed line indicates a Gibbs free energy of zero.

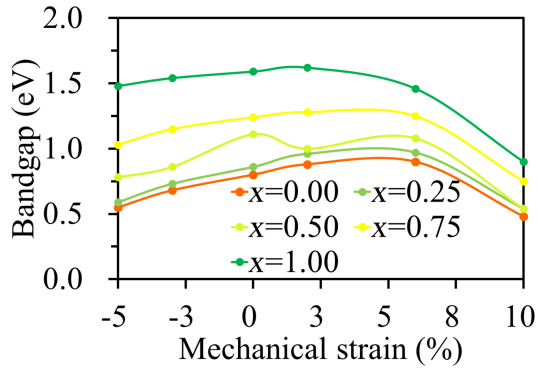

Figure 4: Band gaps of the $SnSe_{2(1-x)}S_{2x}$ monolayers as a function of mechanical strain.

increases upon application of tensile strain because the valence band and conduction band move upward and downward in energy, respectively. Previous reports showed that H adsorption depends on the density of states near the Fermi energy level [57,58], with the adsorption being enhanced as the d-band centre moves closer to the Fermi level. The number of electronic states near the Fermi energy increased with the increasing of tensile mechanical strain, thereby boosting the supply of electrons to the adsorption sites and thus improving the catalytic activity [59]. Figure 5 shows the band structures for SnSeS and $SnSe_{0.5}S_{1.5}$ monolayers with strains of −5%, −3%, 2%, 6% and 10%. As seen from Figure 5, there are fewer valence states near the Fermi energy when compressive strain is applied, and the number of electronic states increases with increasing tensile strain. A higher density of electronic states near the valence-band maximum appears with tensile strain. Moreover, tensile strain caused the valence band to shift upward and the conduction band to shift downward in energy. The results can enhance the interaction between hydrogen and the catalyst. Therefore, the hydrogen-adsorption free energies were decreased from 0.84 to −0.05 eV and from 0.90 to −0.06 eV for H atoms adsorbed on SnSeS and $SnSe_{0.5}S_{1.5}$ at a tensile strain of 10%, respectively. Therefore, applying a suitable tensile strain can efficiently improve the HER efficiency of $SnSe_{2(1-x)}S_{2x}$ monolayers. The tensile strain can be realized by mechanically bending the monolayer $SnSe_{2(1-x)}S_{2x}$ [56].

Conclusion

In conclusion, the electronic properties and catalytic behaviour for HER of $SnSe_{2(1-x)}S_{2x}$ monolayers were investigated using DFT calculations. The band gap of the $SnSe_{2(1-x)}S_{2x}$ monolayer can be continuously tuned from 0.8 eV for $SnSe_2$ to 1.59 eV for SnS_2. The band gap of a $SnSe_{2(1-x)}S_{2x}$ monolayer can be further tuned by applying mechanical strain. Although the basal plane of $SnSe_{2(1-x)}S_{2x}$ monolayer is inert for HER, the mechanical tensile strain provides a direct means to improve the catalytic activity for hydrogen evolution reaction of $SnSe_{2(1-x)}S_{2x}$ monolayer. SnSeS and $SnSe_{0.5}S_{1.5}$ monolayers show the best catalytic activity for HER at a tensile strain of 10%. This work provides a method of improvement of the catalytic activity of $SnSe_{2(1-x)}S_{2x}$ monolayers.

Simulation Details

All calculations were performed based on spin-polarized DFT as implemented in the Vienna ab initio simulation package

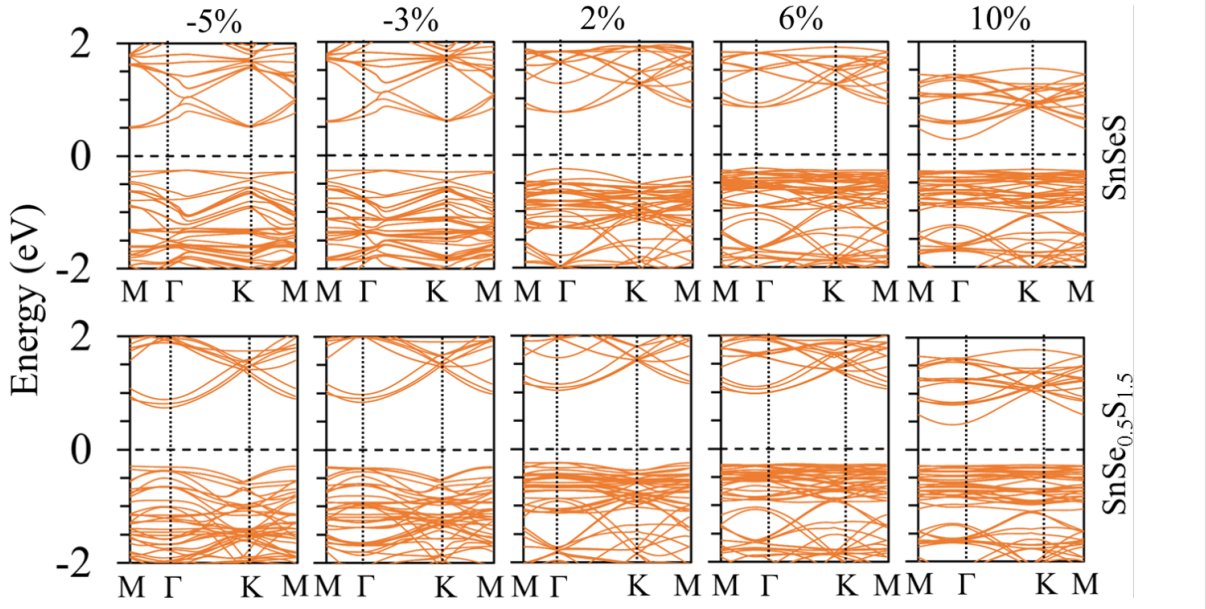

Figure 5: Band structures for SnSeS and $SnSe_{0.5}S_{1.5}$ monolayers with strain of −5%, −3%, 2%, 6% and 10%.

(VASP) [60,61] within the framework of the projector augmented wave method [62]. Electron exchange–correlation was described with the generalized gradient approximation (GGA) within the Perdew–Burke–Ernzerhof (PBE) functional [63]. An energy cutoff of 520 eV was used for the plane-wave basis sets to converge the relevant quantities. The atomic positions and geometric structures were freely relaxed using the conjugate gradient approximation (CG) until the residual force on each atom is less than 0.02 eV·Å^{-1}. A vacuum of 20 Å perpendicular to the monolayer was used to avoid the periodic image interactions.

The HER can be described by Equation 1 under the conditions pH = 0 and $p(H_2)$ = 1bar [64]:

$$H^+_{(aq)} + e^- \longrightarrow \frac{1}{2}H_{2(g)}. \quad (1)$$

The first step of HER is that the H atom is bound to the active site of the catalyst; this step is the rate-determining step [65]. The Gibbs free energy of hydrogen adsorption (ΔG_H) of this step is a key quantity to describe the HER activity of the catalyst; a value of ΔG_H for a good catalyst should be close to zero [66-68]. ΔG_H can be calculated by using Equation 2,

$$\Delta G_H = \Delta E_H + \Delta E_{ZPE} - T\Delta S_H , \quad (2)$$

where ΔE_{ZPE} is the zero-point energy difference between the adsorbed state and the gas phase of hydrogen; because this quantity has a small contribution to ΔG_H, it was neglected in this work. T is the temperature. ΔS_H is the entropy contribution to ΔG_H, which can be approximated as: $\Delta S_H = 1/2 S_{H2}$, where S_{H2} is the entropy of H_2 in the gas phase under standard conditions (300 K, 1 bar) [69]. The approximate value of $\Delta E_{ZPE} - T\Delta S_H$ is 0.38 eV [70,71]. ΔE_H is the hydrogen chemisorption energy and was calculated using Equation 3,

$$\Delta E_H = E_{M+H} - E_M - \frac{1}{2}E_{H2} , \quad (3)$$

where E_{M+H}, E_M, and E_{H2} are the total energy of the catalyst with an adsorbed hydrogen atom, the total energy of the catalyst without adsorption of hydrogen, and the total energy of a molecule of hydrogen, respectively. Using the above values, the Gibbs free energy can be calculated using Equation 4,

$$\Delta G_H = \Delta E_H + 0.38 . \quad (4)$$

Acknowledgements

This work was financially supported by the National Natural Science Foundation of China (11474047) and the Fundamental Research Funds for the Central Universities (ZYGX2016J202). This work was conducted at the National Supercomputer Center in Tianjin, and the calculations were performed on TianHe-1(A).

ORCID® iDs

Zhiguo Wang - https://orcid.org/0000-0002-5652-5362

References

1. Dincer, I.; Acar, C. *Int. J. Hydrogen Energy* **2015,** *40,* 11094–11111. doi:10.1016/j.ijhydene.2014.12.035
2. Burton, L. A.; Whittles, T. J.; Hesp, D.; Linhart, W. M.; Skelton, J. M.; Hou, B.; Webster, R. F.; O'Dowd, G.; Reece, C.; Cherns, D.; Fermin, D. J.; Veal, T. D.; Dhanak, V. R.; Walsh, A. *J. Mater. Chem. A* **2016,** *4,* 1312–1318. doi:10.1039/c5ta08214e
3. Xu, Z.; Ao, Z.; Chu, D.; Younis, A.; Li, C. M.; Li, S. *Sci. Rep.* **2014,** *4,* 6450. doi:10.1038/srep06450
4. Kudo, A.; Miseki, Y. *Chem. Soc. Rev.* **2009,** *38,* 253–278. doi:10.1039/B800489G
5. Khan, S. U. M.; Al-Shahry, M.; Ingler, W. B., Jr. *Science* **2002,** *297,* 2243–2245. doi:10.1126/science.1075035
6. Chen, W.-F.; Iyer, S.; Iyer, S.; Sasaki, K.; Wang, C.-H.; Zhu, Y.; Muckerman, J. T.; Fujita, E. *Energy Environ. Sci.* **2013,** *6,* 1818–1826. doi:10.1039/C3EE40596F
7. Chen, W.-F.; Muckerman, J. T.; Fujita, E. *Chem. Commun.* **2013,** *49,* 8896. doi:10.1039/c3cc44076a
8. Bockris, J. O. M.; Ammar, I. A.; Huq, A. K. M. S. *J. Phys. Chem.* **1957,** *61,* 879–886. doi:10.1021/j150553a008
9. Parsons, R. *Trans. Faraday Soc.* **1960,** *56,* 1340–1350. doi:10.1039/TF9605601340
10. Walter, M. G.; Warren, E. L.; Mckone, J. R.; Boettcher, S. W.; Mi, Q.; Santori, E. A.; Lewis, N. S. *Chem. Rev.* **2010,** *110,* 6446. doi:10.1021/cr1002326
11. Novoselov, K. S.; Jiang, D.; Schedin, F.; Booth, T. J.; Khotkevich, V. V.; Morozov, S. V.; Geim, A. K. *Proc. Natl. Acad. Sci. U. S. A.* **2005,** *102,* 10451–10453. doi:10.1073/pnas.0502848102
12. Li, H.; Pan, L.; Lu, T.; Zhan, Y.; Nie, C.; Sun, Z. *J. Electroanal. Chem.* **2011,** *653,* 40–44. doi:10.1016/j.jelechem.2011.01.012
13. Novoselov, K. S.; Geim, A. K.; Morozov, S. V.; Jiang, D.; Zhang, Y.; Dubonos, S. V.; Grigorieva, I. V.; Firsov, A. A. *Science* **2004,** *306,* 666. doi:10.1126/science.1102896
14. Yang, L.; Majumdar, K.; Liu, H.; Du, Y.; Wu, H.; Hatzistergos, M.; Hung, P. Y.; Tieckelmann, R.; Tsai, W.; Hobbs, C.; Ye, P. D. *Nano Lett.* **2014,** *14,* 6275. doi:10.1021/nl502603d
15. Scalise, E.; Houssa, M.; Pourtois, G.; Afanas'ev, V.; Stesmans, A. *Nano Res.* **2012,** *5,* 43–48. doi:10.1007/s12274-011-0183-0
16. Perea-López, N.; Elías, A. L.; Berkdemir, A.; CastroBeltran, A.; Gutiérrez, H. R.; Feng, S.; Lv, R.; Hayashi, T.; López-Urías, F.; Ghosh, S.; Muchharla, B.; Talapatra, S.; Terrones, H.; Terrones, M. *Adv. Funct. Mater.* **2013,** *23,* 5511–5517. doi:10.1002/adfm.201300760
17. Gao, Y.; Liu, Z.; Sun, D.-M.; Huang, L.; Ma, L.-P.; Yin, L.-C.; Ma, T.; Zhang, Z.; Ma, X.-L.; Peng, L.-M.; Cheng, H.-M.; Ren, W. c. *Nat. Commun.* **2015,** *6,* 8569. doi:10.1038/ncomms9569
18. Huang, Y.; Sutter, E.; Sadowski, J. T.; Cotlet, M.; Monti, O. L. A.; Racke, D. A.; Neupane, M. R.; Wickramaratne, D.; Lake, R. K.; Parkinson, B. A.; Sutter, P. *ACS Nano* **2014,** *8,* 10743. doi:10.1021/nn504481r

19. Ramakrishna Matte, H. S. S.; Gomathi, A.; Manna, A. K.; Late, D. J.; Datta, R.; Pati, S. K.; Rao, C. N. R. *Angew. Chem., Int. Ed.* **2010,** *49,* 4059–4062. doi:10.1002/anie.201000009
20. Zhang, H.; Xia, C.; Zhao, X.; Wang, T.; Li, J. *Appl. Surf. Sci.* **2015,** *356,* 1200–1206. doi:10.1016/j.apsusc.2015.08.213
21. Huang, Y.; Ling, C.; Chen, X.; Zhou, D.; Wang, S. *RSC Adv.* **2015,** *5,* 32505–32510. doi:10.1039/C5RA01211B
22. Huang, Y.; Ling, C.; Liu, H.; Wang, S.; Geng, B. *J. Phys. Chem. C* **2014,** *118,* 9251–9260. doi:10.1021/jp5013158
23. Seo, J.-w.; Jang, J.-t.; Park, S.-w.; Kim, C.; Park, B.; Cheon, J. *Adv. Mater.* **2008,** *20,* 4269–4273. doi:10.1002/adma.200703122
24. Schlaf, R.; Armstrong, N. R.; Parkinson, B. A.; Pettenkofer, C.; Jaegermann, W. *Surf. Sci.* **1997,** *385,* 1–14. doi:10.1016/S0039-6028(97)00066-6
25. Su, Y.; Ebrish, M. A.; Olson, E. J.; Koester, S. J. *Appl. Phys. Lett.* **2013,** *103,* 8983. doi:10.1063/1.4857495
26. Sun, Y.; Cheng, H.; Gao, S.; Sun, Z.; Liu, Q.; Liu, Q.; Lei, F.; Yao, T.; He, J.; Wei, S.; Xie, Y. *Angew. Chem., Int. Ed.* **2012,** *51,* 8727. doi:10.1002/ange.201205557
27. Su, G.; Hadjiev, V. G.; Loya, P. E.; Zhang, J.; Lei, S.; Maharjan, S.; Dong, P.; Ajayan, P. M.; Lou, J.; Peng, H. *Nano Lett.* **2015,** *15,* 506. doi:10.1021/nl503857r
28. Pan, T. S.; De, D.; Manongdo, J.; Guloy, A. M.; Hadjiev, V. G.; Lin, Y.; Peng, H. B. *Appl. Phys. Lett.* **2013,** *103,* 666. doi:10.1063/1.4819072
29. Zhang, Y. C.; Li, J.; Zhang, M.; Dionysiou, D. D. *Environ. Sci. Technol.* **2011,** *45,* 9324. doi:10.1021/es202012b
30. Choi, J.; Jin, J.; Jung, I. G.; Kim, J. M.; Kim, H. J.; Son, S. U. *Chem. Commun.* **2011,** *47,* 5241–5243. doi:10.1039/c1cc10317b
31. Zhang, M.; Wu, J.; Zhu, Y.; Dumcenco, D. O.; Hong, J.; Mao, N.; Deng, S.; Chen, Y.; Yang, Y.; Jin, C.; Chaki, S. H.; Huang, Y.-S.; Zhang, J.; Xie, L. *ACS Nano* **2014,** *8,* 7130–7137. doi:10.1021/nn5020566
32. Xia, C.; An, J.; Wei, S.; Jia, Y.; Zhang, Q. *Comput. Mater. Sci.* **2014,** *95,* 712–717. doi:10.1016/j.commatsci.2014.07.002
33. Su, S.-H.; Hsu, W.-T.; Hsu, C.-L.; Chen, C.-H.; Chiu, M.-H.; Lin, Y.-C.; Chang, W.-H.; Suenaga, K.; He, J.-H.; Li, L.-J. *Front. Energy Res.* **2014,** *2,* 27. doi:10.3389/fenrg.2014.00027
34. Komsa, H.-P.; Krasheninnikov, A. V. *J. Phys. Chem. Lett.* **2012,** *3,* 3652. doi:10.1021/jz301673x
35. Wang, Y.; Huang, L.; Li, B.; Shang, J.; Xia, C.; Fan, C.; Deng, H. X.; Wei, Z.; Li, J. *J. Mater. Chem. C* **2017,** *5,* 84–90. doi:10.1039/C6TC03751H
36. Huang, Y.; Chen, X.; Zhou, D.; Liu, H.; Wang, C.; Du, J.; Ning, L.; Wang, S. *J. Phys. Chem. C* **2016,** *120,* 5839–5847. doi:10.1021/acs.jpcc.6b00794
37. Pei, T.; Bao, L.; Wang, G.; Ma, R.; Yang, H.; Li, J.; Gu, C.; Pantelides, S.; Du, S.; Gao, H.-j. *Appl. Phys. Lett.* **2016,** *108,* 10451. doi:10.1063/1.4941394
38. Liu, H.; Antwi, K. K. A.; Chua, S.; Chi, D. *Nanoscale* **2014,** *6,* 624. doi:10.1039/c3nr04515c
39. Tongay, S.; Narang, D. S.; Kang, J.; Fan, W.; Ko, C.; Luce, A. V.; Wang, K. X.; Suh, J.; Patel, K. D.; Pathak, V. M.; Li, J.; Wu, J. *Appl. Phys. Lett.* **2014,** *104,* 012101. doi:10.1063/1.4834358
40. Duan, X.; Wang, C.; Zheng, F.; Hao, G.; Kou, L.; Halim, U.; Li, H.; Wu, X.; Wang, Y.; Jiang, J.; Pan, A.; Huang, Y.; Yu, R.; Duan, X. *Nano Lett.* **2016,** *16,* 264. doi:10.1021/acs.nanolett.5b03662
41. Fu, Q.; Yang, L.; Wang, W.; Han, A.; Huang, J.; Du, P.; Fan, Z.; Zhang, J.; Xiang, B. *Adv. Mater.* **2015,** *27,* 4732–4738. doi:10.1002/adma.201500368
42. Yue, Q.; Kang, J.; Shao, Z.; Zhang, X.; Chang, S.; Wang, G.; Qin, S.; Li, J. *Phys. Lett. A* **2012,** *376,* 1166–1170. doi:10.1016/j.physleta.2012.02.029
43. Liu, G.; Qiu, Y.; Wang, Z.; Zhang, J.; Chen, X.; Dai, M.; Jia, D.; Zhou, Y.; Li, Z.; Hu, P. *ACS Appl. Mater. Interfaces* **2017,** *9,* 37750–37759. doi:10.1021/acsami.7b11413
44. Meiron, O. E.; Kuraganti, V.; Hod, I.; Bar-Ziv, R.; Bar-Sadan, M. *Nanoscale* **2017,** *9,* 13998–14005. doi:10.1039/c7nr04922f
45. Xu, K.; Wang, F.; Wang, Z.; Zhan, X.; Wang, Q.; Cheng, Z.; Safdar, M.; He, J. *ACS Nano* **2014,** *8,* 8468–8476. doi:10.1021/nn503027k
46. Yang, L.; Wang, W.; Fu, Q.; Zhang, J.; Xiang, B. *Electrochim. Acta* **2015,** *185,* 236–241. doi:10.1016/j.electacta.2015.10.153
47. Topsakal, M.; Cahangirov, S.; Ciraci, S. *Appl. Phys. Lett.* **2010,** *96,* 666. doi:10.1063/1.3353968
48. Benson, E. E.; Miller, E. M.; Nanayakkara, S. U.; Svedruzic, D.; Ferrere, S.; Neale, N. R.; van de Lagemaat, J.; Gregg, B. A. *Chem. Mater.* **2017,** *29,* 2173–2179. doi:10.1021/acs.chemmater.6b04881
49. Yan, K.; Kim, S. K.; Khorshidi, A.; Guduru, P. R.; Peterson, A. A. *J. Phys. Chem. C* **2017,** *121,* 6177–6183. doi:10.1021/acs.jpcc.7b00281
50. Yan, K.; Maark, T. A.; Khorshidi, A.; Sethuraman, V. A.; Peterson, A. A.; Guduru, P. R. *Angew. Chem., Int. Ed.* **2016,** *55,* 6175–6181. doi:10.1002/anie.201508613
51. Liang, D.; Namburu, R. R.; O'Regan, T. P.; Dubey, M.; Dongare, A. M. *J. Mater. Sci.* **2014,** *49,* 6762–6771. doi:10.1007/s10853-014-8370-5
52. Yue, Q.; Chang, S.; Kang, J.; Qin, S.; Li, J. *Int. J. Photoenergy* **2013,** *117,* 14804–14811. doi:10.1021/jp4021189
53. Gao, G.; Jiao, Y.; Ma, F.; Jiao, Y.; Waclawik, E.; Du, A. *J. Catal.* **2015,** *332,* 149–155. doi:10.1016/j.jcat.2015.10.006
54. Denton, A. R.; Ashcroft, N. W. *Phys. Rev. A* **1991,** *43,* 3161. doi:10.1103/PhysRevA.43.3161
55. Putungan, D. B.; Lin, S.-H.; Kuo, J.-L. *Phys. Chem. Chem. Phys.* **2015,** *17,* 21702–21708. doi:10.1039/c5cp03799a
56. Shi, W.; Wang, Z.; Fu, Y. Q. *J. Nanopart. Res.* **2017,** *19,* 296. doi:10.1007/s11051-017-3996-2
57. Ouyang, Y.; Ling, C.; Chen, Q.; Wang, Z.; Shi, L.; Wang, J. *Chem. Mater.* **2016,** *28,* 4390–4396. doi:10.1021/acs.chemmater.6b01395
58. Lin, S.-H.; Kuo, J.-L. *Phys. Chem. Chem. Phys.* **2015,** *17,* 29305–29310. doi:10.1039/c5cp04760a
59. Li, H.; Tsai, C.; Koh, A. L.; Cai, L.; Contryman, A. W.; Fragapane, A. H.; Zhao, J.; Han, H. S.; Manoharan, H. C.; Abild-Pedersen, F.; Norskov, J. K.; Zheng, X. *Nat. Mater.* **2016,** *15,* 364. doi:10.1038/nmat4564
60. Kresse, G.; Hafner, J. *Phys. Rev. B* **1993,** *47,* 558. doi:10.1103/PhysRevB.47.558
61. Kresse, G.; Furthmüller, J. *Comput. Mater. Sci.* **1996,** *6,* 15–50. doi:10.1016/0927-0256(96)00008-0
62. Blöchl, P. E. *Phys. Rev. B* **1994,** *50,* 17953. doi:10.1103/PhysRevB.50.17953
63. Perdew, J. P.; Chevary, J. A.; Vosko, S. H.; Jackson, K. A.; Pederson, M. R.; Singh, D. J.; Fiolhais, C. *Phys. Rev. B* **1992,** *46,* 6671. doi:10.1103/PhysRevB.46.6671
64. Gao, G.; Sun, Q.; Du, A. *J. Phys. Chem. C* **2016,** *120,* 16761–16766. doi:10.1021/acs.jpcc.6b04692
65. Gao, M.-R.; Liang, J.-X.; Zheng, Y.-R.; Xu, Y.-F.; Jiang, J.; Gao, Q.; Li, J.; Yu, S.-H. *Nat. Commun.* **2015,** *6,* 5982. doi:10.1038/ncomms6982

66. Jiao, Y.; Zheng, Y.; Jaroniec, M.; Qiao, S. Z. *Chem. Soc. Rev.* **2015,** *44,* 2060–2086. doi:10.1039/C4CS00470A
67. Schmickler, W.; Trasatti, S. *J. Electrochem. Soc.* **2006,** *153,* L31. doi:10.1149/1.2358294
68. Greeley, J.; Jaramillo, T. F.; Bonde, J.; Chorkendorff, I. B.; Nørskov, J. K. *Nat. Mater.* **2006,** *5,* 909–913. doi:10.1038/nmat1752
69. Voiry, D.; Yamaguchi, H.; Li, J.; Silva, R.; Alves, D. C.; Fujita, T.; Chen, M.; Asefa, T.; Shenoy, V. B.; Eda, G.; Chhowalla, M. *Nat. Mater.* **2013,** *12,* 850–855. doi:10.1038/nmat3700
70. Pandey, M.; Vojvodic, A.; Thygesen, K. S.; Jacobsen, K. W. *J. Phys. Chem. Lett.* **2015,** *6,* 1577. doi:10.1021/acs.jpclett.5b00353
71. Seo, B.; Jung, G. Y.; Sa, Y. J.; Jeong, H. Y.; Cheon, J. Y.; Lee, J. H.; Kim, H. Y.; Kim, J. C.; Shin, H. S.; Kwak, S. K.; Joo, S. H. *ACS Nano* **2015,** *9,* 3728. doi:10.1021/acsnano.5b00786

License and Terms